Mon. Not. R. Astron. Soc. **000**, 000–000 (0000) Printed 27 January 2004 (MN LATEX style file v2.2)

Asteroseismology of the β Cephei star ν Eridani - III extended frequency analysis and mode identification

J. De Ridder[1], J.H. Telting[2], L.A. Balona[3], G. Handler[4], M. Briquet[1], J. Daszyńska-Daszkiewicz [1,5], K. Lefever[1], C. Aerts[1]

[1] *Instituut voor Sterrenkunde, K.U.Leuven, Celestijnenlaan 200B, B-3001 Leuven, Belgium*
[2] *Nordic Optical Telescope, Apartado 474, 38700 Santa Cruz de La Palma, Spain*
[3] *South African Astronomical Observatory, PO Box 9, Observatory 7935, Cape Town, South Africa*
[4] *Institut für Astronomie der Universität Wien, Türkenschanzstr. 17, 1180 Wien, Austria*
[5] *Astronomical Institute of Wrocław University, ul. Kopernika 11, 51-622 Wrocław, Poland*

27 January 2004

ABSTRACT

Using the large photometric and spectroscopic datasets of the ν Eri multi-site campaign (Aerts et al., 2004, and Handler et al., 2004), we present an extended frequency analysis and a photometric mode identification. For the extended frequency analysis we used an improved radial velocity time series, the second moment time series, and the line profiles themselves. In the radial velocity time series, we can now detect an additional pulsation frequency which was previously only found in photometric time series. We also report several new candidate pulsation frequencies. For 7 frequencies the photometric mode identification indicates that they belong to a radial mode and six dipole modes, and for three frequencies the degree ℓ could not be unambiguously determined. We also placed ν Eri in the HR-diagram by determining $T_{\rm eff}$ using Geneva plus Strömgren photometric calibrations, spectral energy distribution fitting, and NLTE Hydrogen and Helium line profile fitting, and by determining $\log L/L_\odot$ using the Hipparcos parallax and a Hβ calibration.

Key words: stars: variables: other – stars: early-type – stars: oscillations – stars: individual: ν Eridani – techniques: spectroscopic – techniques: photometric

1 INTRODUCTION

The massive B-type β Cephei stars are of particular asteroseismic interest. After all, they will be the next generation supernovae, thereby chemically enriching our environment. Modelling their evolution requires, however, a thorough understanding of their convective core and of internal rotational mixing, two topics of which there is currently very limited knowledge. Using low-degree pulsation modes, which have very deep turning points, to probe this convective core currently seems the best way to resolve this problem.

The pulsation periods of β Cephei stars (3-8 h) are, however, significantly longer than those of δ Scuti stars or white dwarfs, making them more challenging targets to detect pulsational frequencies. This is why from October 2002 until January 2003, a large multi-site and multi-technique campaign for a β Cephei star was set up. More than 2000 high-resolution spectra and 3000 photometric measurements in three passbands were obtained for ν Eridani (HD29248, B2III). The data and a frequency analysis are presented in Handler et al. (2004, hereafter Paper Ia), and in Aerts et al. (2004, hereafter Paper Ib). The present paper exploits these datasets further.

Successful seismic modelling not only involves detecting pulsation frequencies, but also mode identifications. Knowing the degree ℓ significantly reduces the number of possible mode matches, and can therefore help narrow down the set of candidate models. In addition, it is essential to know whether we are dealing with an $m = 0$ mode, as the zonal modes are not affected by rotation in the first-order approximation.

In this paper we present the final frequency analysis results (Section 2) of both the spectroscopic and the photometric time series, as well as mode identification results (Section 4). In addition we determined the basic stellar parameters to put ν Eridani in the HR-diagram (see Section

3). These results will serve as the starting point for future stellar modelling papers (Pamyatnykh et al., 2004, in preparation; Ausseloos et al., 2004, in preparation).

2 FREQUENCY ANALYSIS

The time series of ν Eri presented in Papers Ia and Ib are the largest ever collected for a β Cephei star, with the sole purpose to detect as many pulsational frequencies as possible. In what follows we extend the frequency analysis done in the previous papers, by a reanalysis of the radial velocity time series, and for the first time a frequency analysis of the line profile time series.

2.1 The radial velocity

We carefully redetermined the moments (see Aerts et al., 1992, for a definition) of each of the three Si lines of the SiIII triplet around 456 nm. In the intervals [455.0, 455.6] nm, [456.4, 457.2] nm, and [457.2, 457.75] nm around respectively the SiIII 455.3 nm, the SiIII 456.8 nm and the SiIII 457.5 nm line, we first renormalised locally the spectrum and then selected the part which should *not* be regarded as continuum. This part contains the spectral line as well as a bit of continuum that is difficult to distinguish from the far wings of the line. The remaining part of the interval was used to compute the standard deviation σ of the normalised flux noise. The region of the spectrum with points at least 2σ in flux away from the continuum was then extracted as the line profile, of which consequently the normalised moments were computed. The integration boundaries of the moments are thus dynamically determined depending on the S/N ($\equiv \sigma^{-1}$) of the spectrum. The corresponding integration interval is much smaller than the wavelength intervals stated above. The advantage is a considerable noise reduction in the moments time series. As the main mode of ν Eri has a large amplitude (~ 22 km/s), the spectral lines show a rather large periodic Doppler shift. A fixed wavelength integration range would therefore have to be taken quite large to ensure that the entire line profile is always included. But this would also mean the inclusion of noisy continuum on the red side when the line shows a blue shift and vice versa, which degrades the accuracy of the moments.

Note that, as in Paper Ib, we compute the radial velocity with the first moment of the line profile, and not by the central wavelength of a fitted Gaussian, as the Si line profiles are sometimes rather skewed. We also did not use the wavelength of the minimum flux point as this could lead to frequency harmonics in the $v_{\rm rad}$ data regardless of whether the star pulsates linearly or not.

After removing noisy data points (S/N < 150) and outliers, we retained 1740, 1874 and 1827 data points for respectively the SiIII 455.3 nm, 456.8 nm and the 457.5 nm lines. We did a careful frequency analysis of these $v_{\rm rad}$ data and we tabulate the results later in this Section. We find all the "independent" frequencies mentioned in Paper Ib, and in addition we do now find three (instead of only two) frequency peaks of the multiplet around 6.24 d^{-1}. We also find most of the "combination" frequencies stated in Paper Ib, plus some additional ones. Just as in Papers Ia & Ib, we identify a combination frequency as a frequency outside the usual β Cephei frequency interval of [3, 8] d^{-1}, and which can be written as a linear combination of two or more independent frequencies within the estimated observational errors. During multi-frequency solution determinations, these combination frequencies are fixed to their exact linear combination. We realize, however, that this approach is not without risk, as it might not be impossible that a linearly stable high-order eigenfrequency *close to* but not exactly equal to a linear combination frequency might be excited due to non-linear effects. In such a case, fixing the combination frequencies would lead to a biased estimate of the independent frequencies. We nevertheless choose to fix the combination frequencies as it seems unlikely that all or even most of them would be real eigenfrequencies. The alternative, i.e. introducing extra free parameters, would then lead to overfitting and thus to an excessive variance of the estimated independent frequencies.

We made an effort to determine the optimal multi-frequency solution in an N-dimensional box with edges $2\Delta\nu$ around the initial estimate. One way of doing this is to make an N-dimensional grid in the box, with mesh size $\delta\nu$ and verify the performance of the frequency solution in each of the $(2\Delta\nu/\delta\nu + 1)^N$ grid points. This number of grid points is, however, computationally unfeasible for ν Eri for which we have $N = 8$ and $\Delta\nu = 10^{-2}$ d^{-1} and for which we would like to have $\delta\nu = 10^{-4}$ d^{-1}. We therefore resorted to N-dimensional Powell minimisation (see e.g. Press et al., 1992) which we choose because there is no need for derivatives. The function to minimise was the χ^2 function with 8 dependent and 12 combination frequencies in the case of a spectroscopic dataset, and 9 dependent frequencies and 14 combination frequencies in the case of a photometric dataset. This method seemed to perform quite well in a reasonable amount of time. Unfortunately, the window function of the spectroscopic time series has local maxima at $\nu = 0.0023$ d^{-1} and at $\nu = 0.0046$ d^{-1}, which may have led the algorithm to an alias frequency. We therefore also systematically checked whether the frequency combination

$$\{\nu_1 + n_1 \cdot 0.0023, \nu_2 + n_2 \cdot 0.0023, \cdots, \nu_8 + n_8 \cdot 0.0023\},$$

where $\{\nu_i\}$ is the solution after minimisation and $n_i \in \{0, \pm 1, \pm 2\}$, has a better χ^2 value. The results of this optimisation approach are given in Table 1, where we also give for each frequency the amplitude and phase together with their estimated uncertainties.

In fact, one reason for giving Table 1 in addition to Table 2 of both Papers Ia & Ib, is to provide a better feeling of the uncertainties involved. We underline that the error estimates on the frequencies given in papers Ia & Ib are formal estimates (as clearly stated), derived under the assumption of an equidistant time series of a monoperiodic signal with uncorrelated noise. The different values of the derived frequencies for the different Si lines and for the different Strömgren passbands in Table 1 provides another way to assess the uncertainties on the frequencies. The uncertainties on the amplitudes and the phases were computed, as usual, with the local curvature of the χ^2 function where we assumed the frequencies to be known. The derived values of the amplitudes and phases (the latter are not given in papers Ia & Ib) for the different Si lines provide again another view on the uncertainties involved. Especially the

phases seem to be rather inaccurately determined. We note that both the phase and its uncertainty depend on t_0 as well as on the exact value of the frequency.

Concerning the close frequencies around 6.24 d^{-1}, we easily find the frequencies ν_6 and ν_8 in the new radial velocity time series; these were also detected in the photometric time series. The frequency ν_8 is new for the spectroscopic data, as it was not found in the $v_{\rm rad}$ data of Paper Ib. A peak at the position of ν_7 (a frequency which was clearly detected in Paper Ib, and mentioned as a possible *photometric* signal in Paper Ia) is seen in the radial velocity time series of all three Si lines, but shows much less power than mentioned in Paper Ib, as can be read from Table 1. Much of the evidence for ν_7 therefore comes from both Papers Ia and Ib instead of from our new radial velocity time series.

At this point we would like to mention that we did not only do a frequency analysis of the first moment, but also of the second moment $\langle v^2 \rangle$. The motivation to do so is the β Cephei star β Crucis for which some pulsation frequencies were found in the higher moments but not in $\langle v \rangle$ (Aerts et al., 1998), and which were later confirmed by satellite (WIRE) data (Cuypers et al., 2002). However, a frequency analysis of the second moment is notoriously difficult because of the many possible cross-term frequencies. If there are N frequencies ν_i detected in the first moment, there can be $N(N+1)$ frequencies present in the second moment: besides ν_i also $2\nu_i$, $\nu_i+\nu_j$ and $\nu_i-\nu_j$ (Aerts, 1996). In the case of ν Eri this would imply that we can expect 420 frequencies, although not all of them need to have an amplitude above the noise level. The power spectrum of the 2nd moment time series of the SiIII (456.8 nm) line shows indeed many peaks, and we do not list them here for the sake of brevity. The bottom line of our analysis is that besides the many cross-term frequencies, we did not find any convincing new frequencies.

2.2 The line profiles

We continued our quest for frequencies by doing a frequency analysis on the line profiles of the SiIII (455.3 nm) and the SiIII (456.8 nm) lines. Indeed, several examples of β Cephei stars exist for which some pulsation frequencies are clearly detected in the line profiles but not in the radial velocity data (e.g. ε Cen, Schrijvers, Telting & Aerts, 2004).

We considered normalised flux time series at each wavelength point in the intervals [455.16, 455.40] nm and [456.678, 456.922] nm. We used the CLEAN algorithm (Roberts, Lehar & Dreher, 1987) to search for frequencies but systematically verified with classical Fourier analysis that our results are not numerical artifacts. The frequency analysis was done in the interval [0, 30] d^{-1} with a frequency step of 2 10^{-6} d^{-1}. Consequently, we summed the power over all the wavelength bins to obtain an overall power spectrum. The result is shown in Fig. 1. In the corresponding Table 2 we list the 20 frequencies which are clearly present in both silicon line profiles. We also list each time the suspected identification, which is always either one of the independent frequencies also found in the radial velocity, or a linear combination of these independent frequencies. Besides these frequencies we also consider the low amplitude frequencies 4.707 d^{-1} and 4.742 d^{-1} worth to be compared with theoretically predicted frequencies.

Figure 1. The power spectra of the SiIII (455.3 nm) and the SiIII (456.8 nm) line profiles, obtained by summing the power at each wavelength point in the intervals [455.16, 455.40] nm respectively [456.678, 456.922] nm. The power spectra are plotted on top of each other, and can hardly be distinguished. The CLEAN algorithm with gain parameter $g = 0.2$ was used. The thick almost horizontal line denotes the 1σ noise level of the non-CLEAN-ed Fourier power spectrum after prewhitening the time series with the 20 frequencies mentioned in Table 2, and was at each frequency approximated by the average power in a 0.1 d^{-1} interval around that frequency.

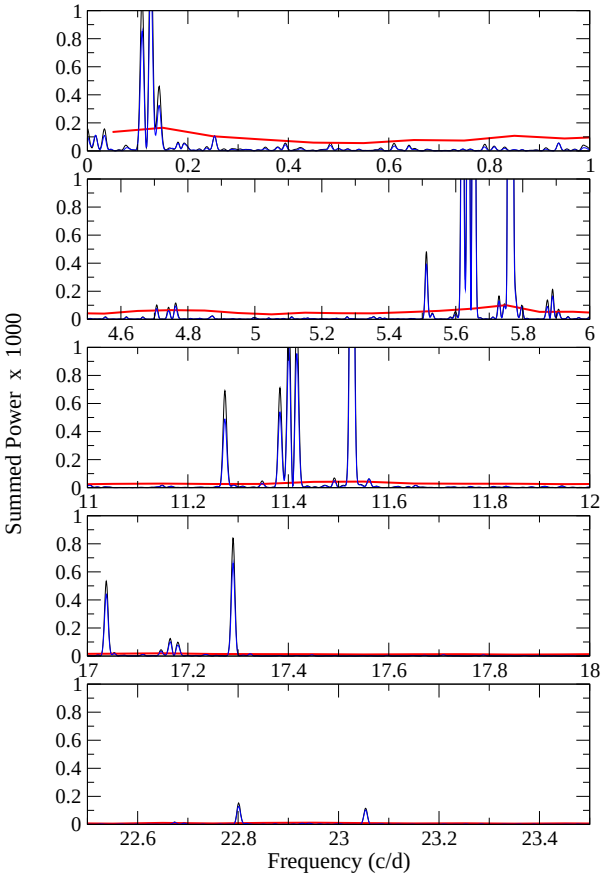

In Table 2 we list two frequency combinations as possible identifications for the frequencies 5.51 d^{-1} and 5.89 d^{-1}. We consequently asked ourselves the following question: as we have 9 genuine eigenfrequencies $\nu_1, \cdots, \nu_9$, shouldn't we expect that about every newly found frequency peak in the β Cephei pulsational frequency range $[\nu_b, \nu_e] = [3, 8]$ d^{-1} can be written as *some* linear combination of these eigenfrequencies? Part of the answer is that it turns out that there are actually not many possible linear combinations that map frequencies from $[\nu_b, \nu_e]$ back into the same interval and that are at the same time not too far-fetched with respect to the linear combinations found in the Fourier spectrum of the radial velocity. Only the general combinations $2\nu_j - \nu_k$ and $\nu_j + \nu_k - \nu_i$ seem to be acceptable. We now compute the probability that a randomly chosen frequency coincides with a combination frequency ν_c. Given n independent frequencies the number of possible combinations $2\nu_j - \nu_k$ is

Table 1. Estimates of the frequencies, amplitudes and phases of the modes found in the radial velocity and the photometric time series. Each frequency was assigned a unique identification. The signal is always written as $C + \sum_{i=1}^{N} A_i \sin(2\pi\nu_i(t-t_0)+\varphi_i)$, where t_0 = HJD2452000. 8 independent and 12 combination frequencies were found in the $v_{\rm rad}$ data, and 9 independent and 14 combination frequencies were found in the photometric data. The combination frequencies were always fixed to their exact linear combination of independent frequencies. The uncertainties on the last given digit of the amplitudes and phases are given between brackets.

	$v_{\rm rad}$ (SiIII 455.3 nm)			$v_{\rm rad}$ (SiIII 456.8 nm)			$v_{\rm rad}$ (SiIII 457.5 nm)		
ID	Freq. (d^{-1})	A (km/s)	φ (deg)	Freq. (d^{-1})	A (km/s)	φ (deg)	Freq. (d^{-1})	A (km/s)	φ (deg)
ν_1	5.76330	22.36(7)	318.0(2)	5.76330	22.50(6)	318.3(2)	5.76330	22.74(6)	318.7(2)
ν_2	5.65396	8.91(9)	69.5(6)	5.65394	9.04(8)	76.5(5)	5.65394	9.09(8)	77.1(5)
ν_3	5.62006	8.11(9)	27.8(6)	5.62006	8.18(8)	29.2(6)	5.62008	8.29(8)	23.6(5)
ν_4	5.63734	7.91(8)	182.8(6)	5.63731	8.00(7)	191.8(5)	5.63731	8.03(7)	191.4(5)
ν_5	7.89845	1.00(7)	307(4)	7.89847	1.00(6)	305(4)	7.89833	0.97(6)	340(4)
ν_6	6.24434	1.03(8)	152(4)	6.24500	1.03(7)	0(4)	6.24510	0.96(7)	335(4)
ν_7	6.22304	0.31(7)	272(15)	6.22099	0.36(6)	55(10)	6.22114	0.35(6)	17(11)
ν_8	6.26080	0.76(8)	86(7)	6.26231	0.76(7)	105(5)	6.26250	0.79(7)	64(5)
ν_{12}	$\nu_1+\nu_3$	2.84(8)	184(2)	$\nu_1+\nu_3$	2.82(8)	183(2)	$\nu_1+\nu_3$	2.84(8)	184(2)
ν_{13}	$\nu_1+\nu_4$	2.59(8)	345(2)	$\nu_1+\nu_4$	2.59(7)	350(2)	$\nu_1+\nu_4$	2.59(8)	345(2)
ν_{14}	$2\nu_4$	0.61(7)	153(7)	$2\nu_4$	0.59(6)	163(6)	$2\nu_4$	0.61(7)	153(7)
ν_{15}	$\nu_1+\nu_2$	3.19(9)	229(2)	$\nu_1+\nu_2$	3.20(8)	233(1)	$\nu_1+\nu_2$	3.19(9)	229(2)
ν_{16}	$2\nu_1$	0.70(7)	96(6)	$2\nu_1$	0.75(6)	97(5)	$2\nu_1$	0.70(7)	96(6)
ν_{17}	$\nu_1+\nu_5$	0.52(7)	93(8)	$\nu_1+\nu_5$	0.48(6)	88(8)	$\nu_1+\nu_5$	0.52(7)	93(8)
ν_{19}	$\nu_1+\nu_2+\nu_3$	1.45(7)	103(3)	$\nu_1+\nu_2+\nu_3$	1.50(6)	108(2)	$\nu_1+\nu_2+\nu_3$	1.45(7)	103(3)
ν_{22}	$2\nu_1+\nu_3$	0.94(8)	351(5)	$2\nu_1+\nu_3$	0.95(8)	347(5)	$2\nu_1+\nu_3$	0.94(8)	351(5)
ν_{23}	$2\nu_1+\nu_4$	0.88(8)	160(5)	$2\nu_1+\nu_4$	0.76(7)	164(5)	$2\nu_1+\nu_4$	0.88(8)	160(5)
ν_{24}	$2\nu_1+\nu_2$	1.14(9)	37(5)	$2\nu_1+\nu_2$	1.11(8)	40(4)	$2\nu_1+\nu_2$	1.14(9)	37(5)
ν_{25}	$3\nu_1$	0.52(7)	178(8)	$3\nu_1$	0.50(6)	169(7)	$3\nu_1$	0.52(7)	178(8)
ν_{26}	$2\nu_1+\nu_2+\nu_3$	0.94(7)	261(4)	$2\nu_1+\nu_2+\nu_3$	0.92(6)	263(4)	$2\nu_1+\nu_2+\nu_3$	0.94(7)	261(4)

	Strömgren u			Strömgren v			Strömgren y		
ID	Freq. (d^{-1})	A (mmag)	φ (deg)	Freq. (d^{-1})	A (mmag)	φ (deg)	Freq. (d^{-1})	A (mmag)	φ (deg)
ν_1	5.76326	73.5(2)	63.4(2)	5.76327	41.0(1)	64.4(2)	5.76327	36.9(1)	63.0(2)
ν_2	5.65391	37.9(2)	172.7(3)	5.65396	26.5(1)	162.0(3)	5.65393	25.1(1)	168.1(3)
ν_3	5.62009	34.6(2)	111.7(3)	5.62007	23.9(1)	117.3(3)	5.62006	22.7(1)	118.4(3)
ν_4	5.63715	32.2(2)	319.8(4)	5.63720	22.4(2)	307.8(4)	5.63718	21.1(1)	313.6(4)
ν_5	7.89757	4.3(2)	246(3)	7.89769	3.1(1)	219(3)	7.89779	2.9(1)	195(2)
ν_6	6.24352	3.9(2)	61(3)	6.24406	2.6(1)	307(3)	6.24326	2.6(1)	114(3)
ν_8	6.26181	2.8(2)	317(4)	6.26178	1.9(1)	322(4)	6.26182	1.7(1)	309(4)
ν_9	7.20012	1.4(2)	109(8)	7.19984	1.0(1)	179(8)	7.19964	1.2(1)	223(6)
ν_{10}	0.43235	5.5(2)	187(2)	0.43190	3.2(1)	289(2)	0.43232	3.2(1)	192(2)
ν_{11}	$\nu_2+\nu_3$	2.8(2)	11(4)	$\nu_2+\nu_3$	1.7(1)	2(5)	$\nu_2+\nu_3$	1.4(1)	2(5)
ν_{12}	$\nu_1+\nu_3$	11.1(2)	297(1)	$\nu_1+\nu_3$	7.9(1)	303(1)	$\nu_1+\nu_3$	7.5(1)	300(1)
ν_{13}	$\nu_1+\nu_4$	10.9(2)	150(1)	$\nu_1+\nu_4$	7.7(2)	139(1)	$\nu_1+\nu_4$	7.1(1)	143(1)
ν_{15}	$\nu_1+\nu_2$	12.6(2)	5.6(9)	$\nu_1+\nu_2$	9.0(1)	354.9(9)	$\nu_1+\nu_2$	8.4(1)	358.8(9)
ν_{16}	$2\nu_1$	4.5(2)	183(3)	$2\nu_1$	3.1(1)	176(3)	$2\nu_1$	2.9(1)	175(3)
ν_{17}	$\nu_1+\nu_5$	1.6(2)	44(7)	$\nu_1+\nu_5$	1.2(1)	15(7)	$\nu_1+\nu_5$	1.1(1)	349(6)
ν_{18}	$\nu_1+\nu_3+\nu_4$	1.0(2)	12(12)	$\nu_1+\nu_3+\nu_4$	0.7(1)	359(12)	$\nu_1+\nu_3+\nu_4$	0.7(1)	15(11)
ν_{19}	$\nu_1+\nu_2+\nu_3$	4.4(2)	256(3)	$\nu_1+\nu_2+\nu_3$	3.1(2)	257(3)	$\nu_1+\nu_2+\nu_3$	2.6(1)	263(3)
ν_{20}	$\nu_1+\nu_2+\nu_4$	1.0(2)	53(13)	$\nu_1+\nu_2+\nu_4$	0.9(1)	30(10)	$\nu_1+\nu_2+\nu_4$	0.9(1)	50(9)
ν_{21}	$\nu_1+2\nu_2$	0.9(2)	257(14)	$\nu_1+2\nu_2$	0.8(1)	236(11)	$\nu_1+2\nu_2$	0.6(1)	253(15)
ν_{22}	$2\nu_1+\nu_3$	1.8(2)	113(7)	$2\nu_1+\nu_3$	1.4(1)	106(6)	$2\nu_1+\nu_3$	1.2(1)	106(6)
ν_{23}	$2\nu_1+\nu_4$	1.8(2)	335(7)	$2\nu_1+\nu_4$	1.2(1)	314(7)	$2\nu_1+\nu_4$	1.1(1)	313(8)
ν_{24}	$2\nu_1+\nu_2$	2.0(2)	181(6)	$2\nu_1+\nu_2$	1.4(1)	162(6)	$2\nu_1+\nu_2$	1.3(1)	166(6)
ν_{26}	$2\nu_1+\nu_2+\nu_3$	1.5(2)	65(7)	$2\nu_1+\nu_2+\nu_3$	1.0(1)	67(8)	$2\nu_1+\nu_2+\nu_3$	0.9(1)	69(8)

simply $n\ (n-1)$, and the number of different combinations $\nu_j+\nu_k-\nu_i$ is $n\ (n-1)\ (n-2)/2$. We consider a frequency to "coincide" with a combination frequency ν_c if it is in the interval $[\nu_c-\delta\nu, \nu_c+\delta\nu]$ with $\delta\nu$ being the observational frequency precision. If n and/or $\delta\nu$ is sufficiently small (as in our case) we can expect that none of these intervals will overlap with another interval. All of these intervals together occupy a fraction

$$\frac{\delta\nu}{\nu_e-\nu_b}\ n^2\ (n-1)$$

of the total β Cephei frequency range $[\nu_b, \nu_e]$, which is equal to the probability that a frequency randomly chosen in this interval falls into one of the intervals. Setting $n=9$, $[\nu_b,\nu_e]=[3,8]$ d^{-1}, and $\delta\nu=10^{-3}$ d^{-1} for the case of ν Eri, we can roughly estimate this probability to be 13%, i.e. a non-negligible probability. We must note, however, that if

Table 2. All frequency peaks which are clearly present in both SiIII (455.3nm) and SiIII (456.8nm) line profiles. We also list the suspected identification, where we used the same notation as in Table 1.

SiIII (455.3nm) Freq. (d^{-1})	SiIII (456.8nm) Freq. (d^{-1})	Possible Identification
0.10880	0.10886	$\nu_1 - \nu_2$
0.12630	0.12622	$\nu_1 - \nu_4$
0.14270	0.14268	$\nu_1 - \nu_3$
5.51228	5.51224	$2\nu_4 - \nu_1$
5.61986	5.61986	ν_3
5.63760	5.63762	ν_4
5.65384	5.65390	ν_2
5.76334	5.76336	ν_1
5.88910	5.88910	$2\nu_1 - \nu_4$
11.27368	11.27364	ν_{11}
11.38330	11.38326	ν_{12}
11.40108	11.40104	ν_{13}
11.41688	11.41688	ν_{15}
11.52670	11.52672	ν_{16}
17.03752	17.03752	ν_{19}
17.16478	17.16480	ν_{23}
17.18004	17.18006	ν_{24}
17.28994	17.28996	ν_{25}
22.80086	22.80086	ν_{26}
23.05362	23.05360	$4\nu_1$

5.51 d^{-1} *is* a genuine eigenfrequency, it should not be regarded as a random frequency as the underlying pulsation physics may impose a higher or a lower probability that it can be written as a linear combination of the other eigenfrequencies.

In fact, in Fig. 2 we find two indications that the frequencies 5.51 d^{-1} and 5.89 d^{-1} might indeed not be combination frequencies. This figure shows the morphology of the amplitude and the phase distribution of several frequencies found in the SiIII (456.8 nm) line profile time series. The amplitudes and phases were computed by fitting the flux time series at each wavelength point with a sum of 20 sines corresponding to the 20 frequencies listed in Table 2. The amplitude and phases of these sines then make up the distributions shown in Fig. 2. We show examples of both genuine eigenfrequencies and known combination frequencies. The phase diagrams of the 5.51 d^{-1} and 5.89 d^{-1} frequencies show a monotonic phase distribution across the line profile with a large phase range. Such behaviour is typical for higher degree modes, which would explain why we don't see the frequencies in the photometry or the radial velocity data. However, this evidence is not conclusive as the combination frequency ν_{11} shows the same phase behaviour in the line profile. Another indication is that for both 5.51 d^{-1} and 5.89 d^{-1} the line profile shows more variability in the line wings than in the line core, which is also systematically true for the eigenfrequencies, while it is vice versa for the combination frequencies. Again, this evidence is not conclusive as we do not know how the velocity distribution of a combination frequency looks like at the surface of the star, so that we also don't know what kind of line profile variations we should expect.

3 BASIC STELLAR PARAMETERS

For a photometric mode identification it is beneficial to have the position of ν Eri in the HR-diagram. This position and its error box can also be used as initial guess and additional constraint for further asteroseismic investigations.

Geneva photometric colours of ν Eri were obtained from the General Catalogue of Photometric Data (Mermilliod et al., 1997). From these colours, the Geneva indices X and Y can be deduced which are independent of interstellar extinction for hot stars like ν Eri. We then used the calibration of Künzli et al. (1997) to obtain $T_{\rm eff} = 23084 \pm 234$ K, and $\log g = 3.88 \pm 0.19$. We emphasise that the uncertainties quoted are lower limits, as the calibration for hot stars requires the metallicity to be known a priori, but we *assumed* it to be solar.

Besides Geneva photometry we also used Strömgren photometry to estimate the effective temperature. We used the large literature survey already done by Hauck & Mermilliod (1998) to obtain the following quantities for ν Eri: $V = 3.960$, $b - y = -0.076$, $m_1 = 0.068$, $c_1 = 0.072$, and $\beta = 2.610$. With these values we can compute the following reddening-free indices:

$$[c_1] = c_1 - 0.2\ (b - y) = 0.087$$

$$[m_1] = m_1 + 0.18\ (b - y) = 0.054$$

$$[u - b] = [c_1] + 2\ [m_1] = 0.196$$

(Strömgren, 1966). Consequently, we used the $[u - b] - T_{\rm eff}$ calibration

$$\frac{5040K}{T_{\rm eff}} = 0.1692 + 0.2828\ [u - b] - 0.0195\ [u - b]^2$$

of Napiwotzki, Schönberner & Wenske (1993) to estimate $T_{\rm eff} = 22500$ K.

Estimating $T_{\rm eff}$ was also done by fitting the spectral energy distribution (SED) of ν Eri. To do so, we collected optical and infrared fluxes of ν Eri from Glushneva et al. (1992), and ultraviolet fluxes from Jamar et al. (1976). It is difficult to estimate to what extend this SED is reddened, but we tried to correct for reddening by using Fitzpatrick's (1999) mean galactic interstellar extinction law. Next, we fitted the dereddened SED with theoretical SEDs computed from LTE Kurucz (1994) stellar atmosphere models. The best fit was obtained for a model with $T_{\rm eff} = 21900$ K. To have an idea about the uncertainty of this value, we examined the effects of varying a little bit the extinction, or the observed UV fluxes (which are most important for our temperature determination) within their observational errors. From this, we roughly estimate the uncertainty to be about 1000 K.

We also used the echelle spectra obtained at the Calar Alto Observatory (see Paper Ib) to make a spectroscopic estimate for $T_{\rm eff}$. We ran the non-LTE FASTWIND code of Santolaya-Rey, Puls & Herrero (1997) to generate a grid of theoretical line profiles of Hα, Hβ, Hγ, HeI (438.7 nm), HeI (447.1 nm), and HeI (492.2 nm). These theoretical line profiles were then compared with the least pulsationally broadened observational line profiles to search for the $T_{\rm eff}$, $\log g$, and the particle number ratio $n({\rm He})/n({\rm H})$ for which the match is best. We verified that the pulsational broadening does not affect our results. The comparison was first done for solar He content: $n({\rm He})/n({\rm H}) = 0.10$. For this chemical composition no ($T_{\rm eff}$, $\log g$) combination could be found for which

Figure 2. Amplitude and phase distributions for several frequencies, for the the SiIII (456.8 nm) line. On the left hand side the distributions of the genuine eigenfrequencies plus the frequencies 5.51 d^{-1} and 5.89 d^{-1} are shown. For comparison, we also show the distributions of some combination frequencies, on the right hand side. The amplitudes are unitless as the line profiles are normalised. The phases are expressed in radians.

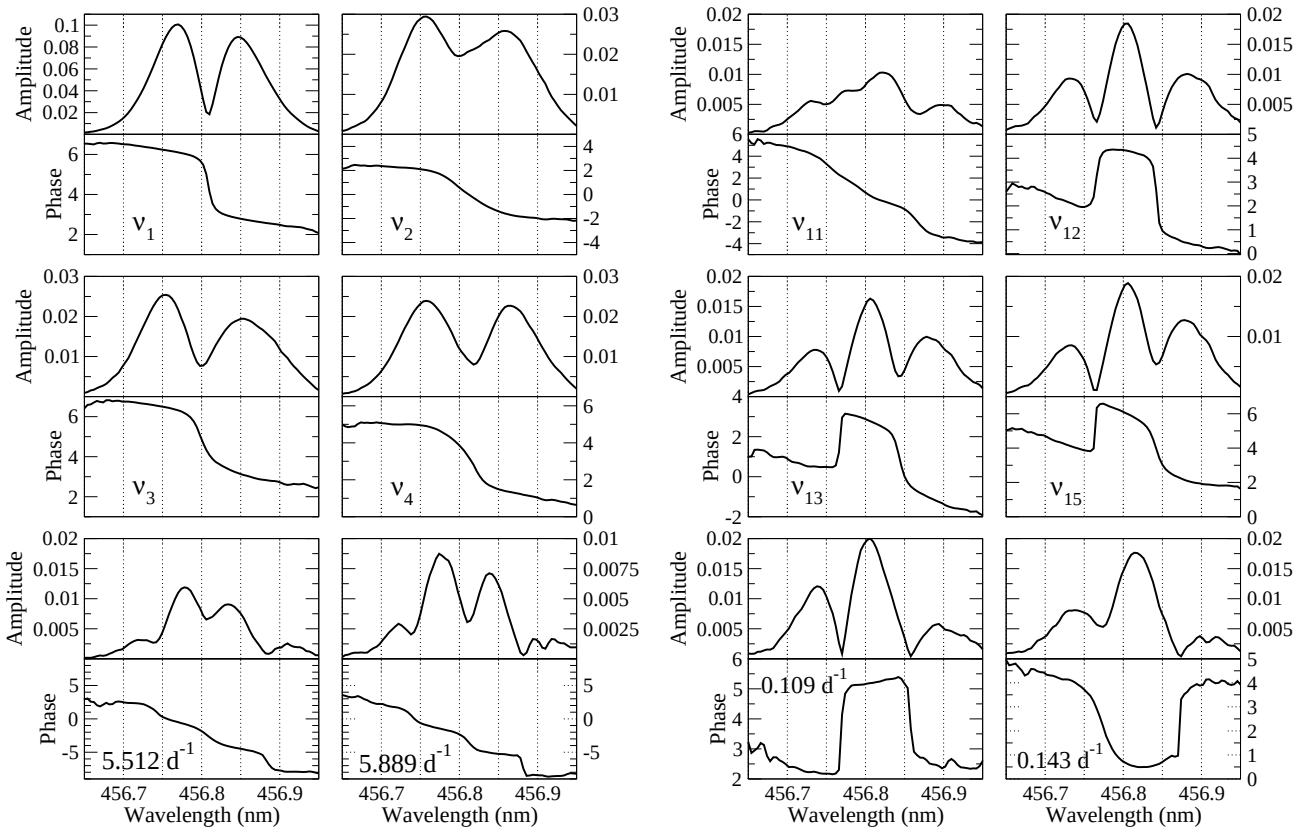

it is possible to fit *both* the H and the He lines satisfactorily. We were forced to try higher He abundances and found a satisfying match for $n(\mathrm{He})/n(\mathrm{H}) = 0.15$: $T_{\rm eff} = 21000$ K and $\log g = 3.4$, which we show in Fig. 3. For the same enhanced He content, it is possible to go to somewhat higher $T_{\rm eff}$ and $\log g$ values and still have acceptable fits, although not as good as the one shown. This leads us to roughly estimate the uncertainties of $T_{\rm eff}$ and $\log g$ to be 1500 K, respectively 0.2 dex. The fact that we seem to find a He overabundance is not too surprising as the chemical analysis of Kilian (1992) shows that half of her sample of unevolved B-stars are actually He overabundant. The very slow rotation of ν Eri (see Paper Ib) is in fact consistent with our findings in the sense that Zboril & North (1999) show that He enhanced B-stars are significantly slower rotators than normal B-type stars. We are, however, surprised to find a good fit for a $\log g$ as low as 3.4. This would imply a post-MS evolution stage for ν Eri, which is incompatible with the observed frequencies as will be shown by Pamyatnykh et al. (2004, in preparation) and Ausseloos et al. (2004, in preparation). We do not have a solid explanation for this, but a search in the literature revealed that ν Eri is not an isolated case. Leone & Lanzafame (1998) encounter similar suspiciously low spectroscopically determined $\log g$ values for the β Cephei stars γ Peg and δ Ceti. In any case, our spectroscopically derived parameters should be treated cautiously. If there is indeed a He enhancement, the same should be said about the photometrically derived parameters, as Zboril et al. (1997) show that not taking into account the effects of He enhancement leads to overestimated photometrically determined $T_{\rm eff}$ values.

Following the discussion above, we adopt conservatively $T_{\rm eff} = 22000 \pm 1500$K, in the hope that the true value is indeed contained in this rather large interval.

In order to compute the luminosity from the visual magnitude V we first need to compute the interstellar extinction A_V. Although A_V is very difficult to estimate, we are somewhat fortunate that the galactic latitude $b = -31^\circ$ of ν Eri implies that the star does not lie in the patchy galactic plane, so that we can make a rough estimate of A_V with the work of Sandage (1972). This leads to $A_V \approx 0.2$, and thus to $V_0 \approx 3.76$. The Hipparcos parallax $\pi = 5.56 \pm 0.88$ mas implies a distance $d = 180 \pm 28$ pc. The absolute visual magnitude is therefore $M_{V_0} = -2.52 \pm 0.34$ where we assumed that most of the uncertainty on M_{V_0} comes from the uncertainty on the distance rather than from the uncertainty on the dereddened V_0 magnitude. From the work of Flower (1996) we derive a bolometric correction of BC $= -2.12 \pm 0.16$ where the uncertainty comes from the un-

Figure 3. Observational Hydrogen and Helium line profiles (coloured) together with their best fits (black) which were obtained for $T_{\rm eff}$ = 21000 K, $\log g$ = 3.4, and n(He)/n(H) = 0.15. The arrow points to a well known (Grigsby, Morrison & Anderson, 1992) temperature sensitive forbidden HeII component which was also considered during the fitting.

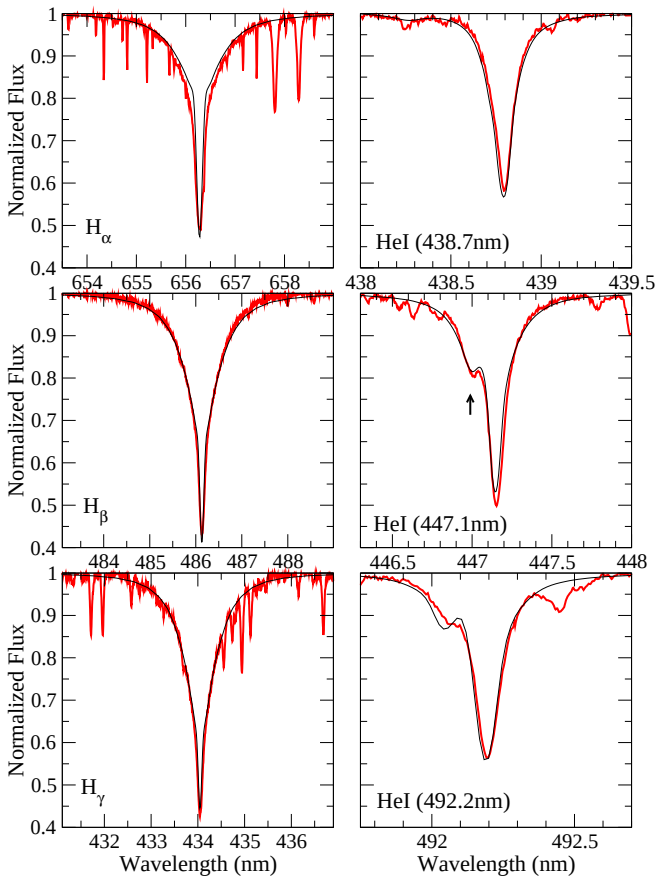

certainty on $T_{\rm eff}$. This leads to $M_{\rm bol} = -4.64 \pm 0.38$ and thus to $\log(L/L_\odot) = 3.76 \pm 0.15$. The position of ν Eri in the HR diagram with the previously derived $T_{\rm eff}$ and $\log(L/L_\odot)$ estimates, is shown in Fig. 4. Another way to estimate the luminosity is to use the strength of the Hβ Balmer line as measured by the Strömgren β index. We applied the Hβ luminosity calibration of Balona & Shobbrook (1984), and obtained $M_{V_0} = -3.16 \pm 0.40$ and therefore $M_{\rm bol} = -5.28 \pm 0.43$ and $\log(L/L_\odot) = 4.01 \pm 0.17$, different but not incompatible with our value obtained with the Hipparcos parallax.

Having two independent estimates for the luminosity, we adopt conservatively the mean value and the union of the error boxes: $\log(L/L_\odot) = 3.89 \pm 0.29$. The uncertainty of the luminosity is therefore rather large. This will be relevant to determine in which overtone the modes of ν Eri pulsate (Pamyatnykh et al., 2004; Ausseloos et al., 2004, both in preparation).

Figure 4. The estimated position and uncertainty box of ν Eri in the HR diagram, assuming that ν Eri has a solar chemical composition. Synthetic evolutionary tracks are drawn in thin full lines, the zero-age and the terminal-age main sequences in thick full lines, and the theoretical β Cephei instability strip for ℓ up to 2 in a thick dashed line. Except for the evolutionary tracks, which we computed ourselves, the sequences and the strip were taken from Pamyatnykh (1999). They were computed with X = 0.7, Z = 0.02, a mixing length parameter α = 1.0, and without taking into account the effects of convective core overshooting and rotation. We refer to Pamyatnykh (1999) for more details on this instability strip.

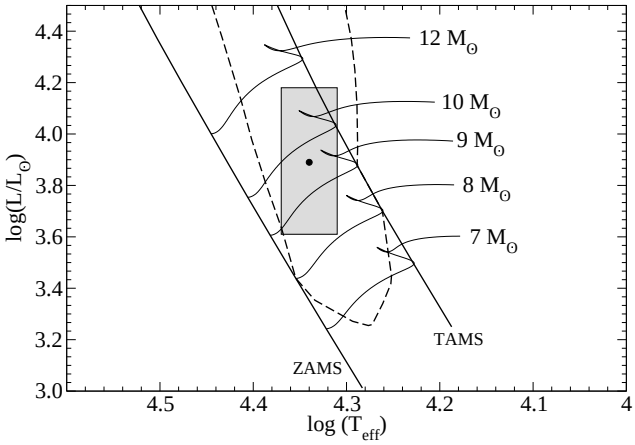

4 MODE IDENTIFICATION

We used the well-known method of photometric amplitude ratio fitting to determine the degree ℓ of each mode (see e.g. Cugier, Dziembowski & Pamyatnykh (1994), and Balona & Evers (1999)). The observational amplitude ratios (normalised w.r.t. the u filter) were computed from Table 1 for the nine independent frequencies. To compute the theoretical amplitude ratios, we used the Liège stellar evolution code CLES and the non-adiabatic pulsation code MAD (Dupret, 2001) to compute the required nonadiabatic parameters, together with Kurucz (1994) atmosphere models. First we computed a series of models in the error box determined in Section 3. From each of these models we then extracted all modes with $0 \leqslant \ell \leqslant 4$ in the frequency range [5.5, 8] d^{-1}, except for the low-frequency mode ν_{10} for which we used the frequency range [0.3, 0.55] d^{-1}. For each of these modes, we computed the photometric amplitude ratios, and finally we took the average of these ratios and compared them with the observational ratios. To have an idea about the uncertainty of the theoretical amplitude ratios we also computed the rms scatter which allows us to define a minimal uncertainty region. The comparison between the theoretical and observational photometric amplitude ratios is shown in Fig. 5. We systematically omitted the theoretical $\ell = 3$ amplitude ratios as their peculiar wavelength dependence is easily recognised but not seen in the data. In addition, for $\ell = 3$ modes one expects very low light curve amplitudes due to a considerable surface cancellation effect. From Fig. 5 we see that ν_1 is clearly a radial mode and that ν_2, ν_3 and ν_4 are components of an $\ell = 1$ triplet. Also ν_5 is clearly an $\ell = 1$ mode. For ν_6 and ν_8 there might be some doubt between $\ell = 0$ and $\ell = 1$ but from theoretical frequency spectra we know that no radial mode can be as close to the radial mode ν_1

Figure 5. Observed (bullets with error bars) and theoretical *uvy* amplitude ratios (lines) for ν Eri. All amplitudes are normalised w.r.t. the u filter. Full lines are radial modes, dotted lines are ℓ=1 modes, dashed lines are ℓ=2 modes, and dashed-dotted lines are ℓ=4 modes. The grey regions are the minimal uncertainty regions for the theoretical amplitude ratios, computed with the rms scatter of amplitude ratios of the different models in the error box in the HR-diagram. The frequency identifications are the same as in Table 1.

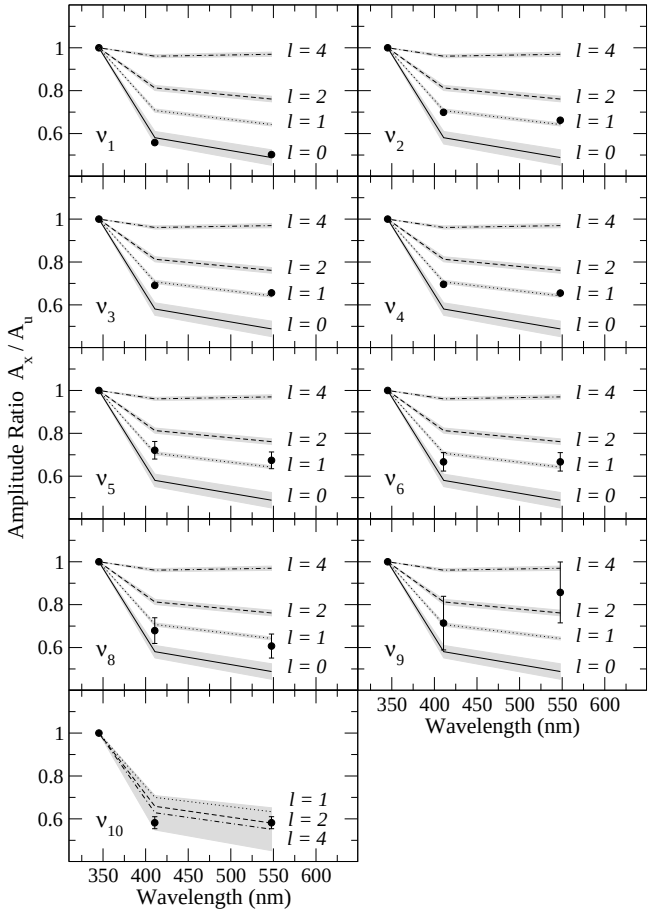

as ν_6 and ν_8 are. This implies that ν_6 and ν_8 are also $\ell = 1$ modes. No clear photometric mode identification is possible for ν_9 as its amplitude is too small. In the panel of the low-frequency mode ν_{10} it can be seen that the rms scatter of the theoretical amplitude ratios is rather large. Moreover, this rms scatter is larger for higher degree ℓ. The uncertainty regions of the $\ell = 1$ and $\ell = 2$ are still disjunct, but the uncertainty region of $\ell = 4$ overlaps both of them. The comparison with the observational amplitude ratios points towards an $\ell = 2$ or an $\ell = 4$ mode, although an $\ell = 1$ mode cannot be firmly excluded. As we verified, including models with higher luminosity does not alter any of our results, so the mode identification is robust with respect to the exact size of the error box. This is not a surprise, because all unstable modes within the β Cephei instability strip are grouped in well separated regions of different degrees ℓ, as was shown by Cugier et al. (1994).

The photometric mode identification method outlined above features the characterisation of an "average" radial mode, an "average" dipole mode etc. This was done by computing the mean and the rms of theoretical amplitude ratios of all relevant modes of all stellar models in the error box in the HR diagram. We will now adopt a complementary approach where we search for the stellar model that fits best the photometric observations (in the χ^2 sense) but without trying to fit the observed frequency values themselves. Besides the photometric amplitude ratios A_v/A_u and A_y/A_u, we also fitted the photometric phase differences $\varphi_v - \varphi_u$ and $\varphi_y - \varphi_u$, and computed the χ^2 in the usual way. Given the errors on the photometric amplitudes and phases, the errors on the amplitude ratios and phase differences were computed assuming that measurements in different passbands are independent. This time the stellar models in the error box in the HR diagram were computed with the Warsaw-New Jersey stellar evolution code, and the non-adiabatic eigenfunctions with the pulsation code of Dziembowski (1977). We also allowed for variations in metallicity ($Z \in [0.015, 0.023]$) but we still neglected the effects of overshooting. The diagrams with χ^2 as a function of the degree ℓ for the best model are shown in Figure 6. This model has a mass $M = 9M_\odot$, a metallicity $Z = 0.016$ and an effective temperature $T_{\rm eff} = 22500$ K. It is reassuring to find essentially the same results as before. The main mode ν_1 is clearly a radial mode and modes ν_2 up to ν_8 and ν_{10} are best explained with dipole modes. The frequency ν_9 seems, however, to be best fitted with a degree ℓ higher than one.

One of the important differences between the two photometric mode identifications we presented, is the selection of the modes. Figure 5 is based on both stable and unstable modes, while Figure 6 is based on unstable modes only (except for ν_{10} for which we could only find stable modes). Stable modes are usually disregarded for a photometric mode identification, but for ν Eri we make an exception. As will be shown by Pamyatnykh et al. (2004, in preparation) and by Ausseloos et al. (2004, in preparation) the observed frequency values strangely cannot be explained with standard stellar models if one only considers unstable modes. We therefore included also stable modes for Figure 5, but disregarded them for Figure 6 to see to what extend the results would be altered. The important conclusion is that both approaches lead to the same mode identification. The contrast between the fairly good fits on Figure 5 with the sometimes considerably large χ^2 values in Figure 6 (especially for ν_1, although difficult to see on the Figure) is also explained by the selection of the modes.

For the modes $\nu_1, \cdots, \nu_4$ and the modes ν_6 and ν_8, we can be fairly confident about their degree ℓ as well as their azimuthal order m. Of the remaining frequencies for which we still need information, only ν_7 is also present in the spectroscopic data. To gain extra information about this frequency, and about the frequencies 5.51 d^{-1} and 5.89 d^{-1} we attempted a spectroscopic mode identification by modelling the moments, the amplitude and phase distributions, and the line profiles. For all three techniques we encountered the problem of the enormous amount of computing power required to reliably and usefully model such a large spectroscopic time series containing so many frequencies. Modelling subsets of this time series did not allow to resolve the interesting frequencies. One of the difficulties is that it is not possible to identify and "remove" the modes one by one, as the effects of the different modes on the line profiles are coupled, much in contrast with the case of the photometric time

Figure 6. χ^2 diagrams for the model that fits best the observed photometric amplitude ratios and phase differences. This model has parameters $M = 9M_\odot$, $Z = 0.016$ and $T_{\rm eff} = 22500$ K. For each mode observed in the photometric time series of Handler et al. (2004), the χ^2 value is shown as a function of the degree ℓ. The frequency identifications are the same as in Table 1.

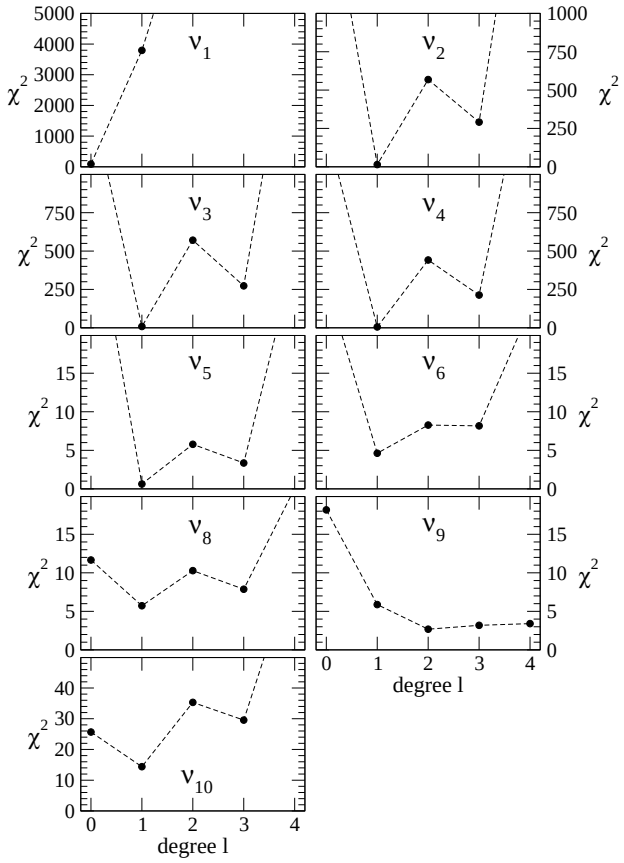

series. We actually tried the one-by-one procedure with line profile fitting by binning the line profiles with the frequency with the highest amplitude, then identifying the mode by fitting a one-mode model, and consequently removing the mode by fitting a sinusoid to the line intensity variations at each wavelength and subtracting it from the data. We checked this procedure for the four main modes, for which we already know the wave numbers, but the results were rather discouraging. To fit the amplitude and phase distributions, we worked initially with a model with four modes. We used both a simple but fast line profile model with a Gaussian intrinsic profile, as well as PULSTAR (De Ridder et al., 2002) which is slower but uses more advanced Kurucz intensity spectra. We did not succeed, however, to find a reliable fit to the observed amplitude and phase distributions. For ν_2, ν_3, and ν_4 this is mainly due to the fact that all three modes have a phase distribution with a negative slope (cf. Fig. 2), which would indicate that they are all prograde, which should not be the case for a dipole triplet. From a spectroscopic point of view, the frequencies around ν_4 are more likely explained by three peaks of an $\ell = 2$ quintuplet with azimuthal orders $m = 0$, $m = -1$, and $m = -2$. In this sense there is a clear but unexplained discrepancy between the spectroscopic and the photometric mode identification for the frequencies ν_2, ν_3, and ν_4.

5 SUMMARY AND CONCLUSIONS

We can now summarize the observational results of the 2003 multi-site and multi-technique campaign of the β Cephei star ν Eridani.

According to the photometric mode identification, we find in the radial velocity time series a high-amplitude radial mode ν_1, a dipole triplet $\nu_2, \cdots, \nu_4$, two close dipole modes ν_6 and ν_8 likely to be part of the same triplet, and yet another dipole mode ν_5 of which we are, however, uncertain whether it is a zonal or a sectoral mode. The degree ℓ of the frequency ν_7 could not be determined, and it is therefore uncertain whether it belongs to the same dipole triplet of ν_6 and ν_8. In addition to the frequencies just mentioned, two other significant frequency peaks (ν_9 and ν_{10}) are found in all three observed Strömgren passbands, although we were unable to determine uniquely their degrees ℓ. Concerning the low-frequency peak ν_{10}, we explicitly checked again if we could find it in the improved radial velocity time series, but with no positive result. This may cast some doubt whether this frequency is indeed a genuine eigenfrequency. The reasons why we included it nevertheless in Table 1 were given in Paper Ia and can be summarised as follows. First, this frequency appears in all three photometric filters. Secondly, its amplitude is far above the noise level. In fact, we find at least 3 eigenfrequencies with lower amplitudes in the photometry. Thirdly, in Paper Ia it is explicitly checked that the variability at this frequency is not due to the comparison stars μ Eri or ξ Eri. Fourthly, in the same paper it was also checked that this frequency is not a (reasonable) combination frequency. And fifthly, the frequency is also detectable in the datasets of the individual observatories.

For the rotationally split multiplet around 5.63 $\rm d^{-1}$ we obtained the following frequency differences: $\nu_4 - \nu_3 = 0.01718(9)$ $\rm d^{-1}$, $\nu_2 - \nu_4 = 0.01669(7)$ $\rm d^{-1}$. For the frequencies around 6.24 $\rm d^{-1}$ we obtained the differences: $\nu_8 - \nu_6 = 0.0171(5)$ $\rm d^{-1}$ and $\nu_6 - \nu_7 = 0.021(3)$ $\rm d^{-1}$. The uncertainty on the last mentioned decimal place is given between brackets, and was estimated from the scatter between the different values obtained from the different spectral lines and the different Strömgren passbands.

The list of combination frequencies found in the photometric time series is not the same list of combination frequencies found in the improved radial velocity time series, which is in turn not exactly the same as the list of combination frequencies found in the radial velocity time series of Paper Ib, although there is a great deal of overlap in all three lists. The common property of all combination frequencies is, however, that they never include a *difference* of two independent frequencies.

In the line profiles a few other candidate frequencies were found in the β Cephei frequency range. They are not certain enough to be included in a seismic modelling of ν Eri but might be used to gain extra confidence in a model if this model turns out to be compatible with these candidate frequencies.

ACKNOWLEDGEMENTS

We thank R. Scuflaire for the use of the stellar evolution code CLES, and M.-A. Dupret for the use of the non-adiabatic pulsation code MAD. We thank W. Dziembowski and A. Pamyatnykh for the use of the Warsaw-New Jersey stellar evolution and pulsation codes. We thank M. Ausseloos for a careful reading of the manuscript. JDR and MB are Postdoctoral Fellows of the Fund for Scientific Research, Flanders. GH's work is supported by the Austrian Fonds zur Förderung der wissenschaftlichen Forschung under grant R12-N02. This study was made possible thanks to support of the Research Fund K.U.Leuven under grant number GOA/2003/04.

REFERENCES

Aerts C., de Pauw M., Waelkens C., 1992, A&A, 266, 294
Aerts C., 1996, A&A, 314, 115
Aerts C., De Cat P., Cuypers J., Becker S.R., Mathias P., De Mey K., Gillet D., Waelkens C., 1998, A&A, 329, 137
Aerts C. et al., 2004, MNRAS, 347, 463 (Paper Ib)
Balona L.A., Shobbrook R.R., 1984, MNRAS, 211, 375
Balona L.A., Evers E.A., 1999, MNRAS, 302, 349
Cugier H., Dziembowski W.A., Pamyatnykh A.A., 1994, A&A, 291, 143
Cuypers J., Aerts C., Buzasi D., Catanzarite J., Conrow T., Laher R., 2002, A&A, 392, 599
De Ridder J., Dupret M.-A., Neuforge C., Aerts C., 2002, A&A, 385, 572
Dupret M.-A., 2001, A&A, 366, 166
Dziembowski W., 1977, Acta Astr., 27, 203
Fitzpatrick E.L., 1999, PASP, 111, 63
Flower P.J., 1996, ApJ, 469, 355
Glushneva I.N., Kharitonov A.V., Kniazeva L.N., Shenavrin V.I., 1992, A&AS, 92, 1
Grigsby J.A., Morrison N.D., Anderson L.S., 1992, ApJSS, 78, 205
Handler G., Shobbrook R.R., Jerzykiewicz M., et al., 2004, MNRAS, 347, 454 (Paper Ia)
Hauck B., Mermilliod M., 1998, A&AS, 129, 431
Jamar C., Macau-Hercot D., Monfils A., Thompson G.I., Houziaux L., Wilson R., 1976, *Ultraviolet bright-star spectrophotometric catalogue. A compilation of absolute spectrophotometric data obtained with the Sky Survey Telescope (S2/68) on the European Astronomical Satellite TD-1*
Kilian J., 1992, A&A, 262, 171
Künzli M., North P., Kurucz R.L., Nicolet B., 1997, A&AS, 122, 51
Kurucz R.L., 1994, *Solar abundance atmospheres*, CD-ROM No. 19, Smithsonian Astrophysical Observatory, Cambridge, Mass.
Leone F., Lanzafame A.C., 1998, A&A, 330, 306
Napiwotzki R., Schönberner D., Wenske V., 1993, A&A, 268, 653
Pamyatnykh A.A., 1999, Acta Astr., 49, 119
Press W.H., Teukolsky S.A., Vetterling W.T., Flannery B.P., 1992, *Numerical Recipes in C. The art of scientific computing*, 2nd edition, Cambridge University Press
Roberts D.H., Lehar J., Dreher J.W., 1987, AJ, 93, 968
Sandage A., 1972, ApJ, 178, 1
Santolaya-Rey A.E., Puls J., Herrero A., 1997, A&A, 323, 488
Schrijvers C., Telting J.H., Aerts C., 2004, A&A, in press
Strömgren B., 1966, Ann. Rev. Astron. Astrophys., 4, 433
Vuille F., 2000, MNRAS, 313, 179
Zboril M., North P., 1999, A&A, 345, 244
Zboril M., North P., Glagolevskij Y.V., Betrix F., A&A, 324, 949

This paper has been typeset from a TEX/ LATEX file prepared by the author.